

RESEARCH

Open Access



Functional and structural characterization of the human indolethylamine *N*-methyltransferase through fluorometric, thermal and computational docking analyses

Matteo Ardini^{1*}, Francesco Angelucci¹, Francesca Rea¹, Luca Paluzzi^{1,2}, Federica Gabriele¹, Marta Palermo^{1,2}, Luana Di Leandro¹, Rodolfo Ippoliti^{1*} and Giuseppina Pitari¹

Abstract

Background The “psychedelic renaissance” is sparking growing interest in clinical research, along with a rise in clinical trials. Substances such as 3,4-methylenedioxymethamphetamine (MDMA), psilocybin and *N,N*-dimethyltryptamine (DMT) are involved. The focus of this paper is on indolethylamine *N*-methyltransferase (INMT), a crucial enzyme in the biosynthesis of key compounds, including DMT, which meets science, medicine and spirituality. The presence of DMT in animals and plants raises many questions about its biological role. Meanwhile, the distribution of INMT in various organs and its involvement in diseases like cancer and mental disorders also fuel investigations worldwide. However, INMT remains largely unexplored, particularly its enzymatic mechanism and structural properties, leaving a significant gap in potential applications.

Results This study examines for the first time the catalytic activity of the human INMT (hINMT) using a simple fluorometric steady-state assay employing the substrate quinoline. The findings are supported by thermal shift and docking analyses, providing valuable information about optimal chemical conditions and potential binding sites for substrates. The thermal shift assays indicate that recombinant hINMT is unstable and requires acidic or near-neutral pH and low salt levels. These experiments also allow for the estimation of dissociation constants for its natural coenzymes SAM and SAH, helping to determine the appropriate setup for the fluorometric assays and calculate kinetic constants, which are comparable to other methyltransferases. The docking indicates that quinoline occupies the same site as the natural substrate tryptamine, further validating the fluorometric approach.

Conclusions The paper provides a foundation for thoroughly studying hINMT under consistent conditions, which is crucial for obtaining reliable kinetic data and maintaining molecular stability for future structural analysis. This represents a valid alternative over previous endpoint radioactive-based and chromatography-mass spectrometry assays, which can provide only apparent steady-state parameters. Given the polymorphisms observed in hINMT and their potential association with psychiatric disorders, e.g., schizophrenia, and cancer, this strategy could serve as an invaluable tool for understanding the structure–function relationship of enzyme mutants and their role in diseases.

*Correspondence:

Matteo Ardini
matteo.ardini@univaq.it
Rodolfo Ippoliti
rodolfo.ippoliti@univaq.it

Full list of author information is available at the end of the article



© The Author(s) 2025. **Open Access** This article is licensed under a Creative Commons Attribution-NonCommercial-NoDerivatives 4.0 International License, which permits any non-commercial use, sharing, distribution and reproduction in any medium or format, as long as you give appropriate credit to the original author(s) and the source, provide a link to the Creative Commons licence, and indicate if you modified the licensed material. You do not have permission under this licence to share adapted material derived from this article or parts of it. The images or other third party material in this article are included in the article's Creative Commons licence, unless indicated otherwise in a credit line to the material. If material is not included in the article's Creative Commons licence and your intended use is not permitted by statutory regulation or exceeds the permitted use, you will need to obtain permission directly from the copyright holder. To view a copy of this licence, visit <http://creativecommons.org/licenses/by-nc-nd/4.0/>.

Furthermore, these findings for the first time provide insights into the interaction modalities of hINMT with its substrates and lay the groundwork for inhibition experiments aimed at practical applications.

Keywords Psychedelic, Indolethylamine *N*-methyltransferase assay, Quinoline, *S*-adenosylmethionine

Background

Methylases or methyltransferases (MTs), the enzymes responsible for the addition of methyl groups (CH₃) to various substrates, play pivotal roles in biological processes ranging from gene expression regulation to cellular signaling. These enzymes catalyze the transfer of methyl groups from *S*-adenosylmethionine (SAM) to specific targets, including DNA, RNA, proteins, and small molecules [57].

Among the others, indolethylamine *N*-methyltransferase (INMT, EC 2.1.1.49) is a crucial enzyme involved in the biosynthesis of various neuroactive molecules within the human body. INMT belongs to class I MTs and catalyzes the methylation of indolethylamine compounds, tryptamine and structurally related substances such as serotonin, to produce *N*-methyltryptamine (NMT), *N,N*-dimethyltryptamine (DMT), and *N*-methylserotonin (NMS) [56]. It is shown that the enzyme also possesses Selenium- and Tellurium-methyltransferase activity [26, 39, 68, 64].

DMT, a naturally occurring psychedelic in mammals, is biosynthesized via aromatic-L-amino acid decarboxylase (AADC) and INMT enzymes [20]. Belonging to the tryptamine family, DMT occurs also in various plant species, including *Psychotria viridis*, essential component of ayahuasca, a traditional entheogenic brew [8]. Research explores its effects on consciousness and potential therapeutic uses for depression, anxiety, and addiction [10]. As our understanding grows, DMT provides insight into the interplay of chemistry, consciousness, and spirituality.

Several hypotheses have emerged regarding the physiological role of endogenous DMT, such as its function as an immunomodulator or involvement in altered states of consciousness similar to schizophrenia [50], although a clear relationship between DMT and altered states of consciousness has not yet been established [9, 31], primarily due to the challenges in fully characterizing the enzymatic properties of INMT. However, it is possible to link alterations in specific genes with behavioral phenotypes. For instance, single nucleotide polymorphisms (SNPs) in INMT could influence the synthesis and thus the endogenous levels of DMT, generating altered states in the individual [21]. Furthermore, emerging evidence suggests that INMT may have broader implications beyond its role in neurotransmitter metabolism, with potential links to psychiatric

disorders, neurodegenerative diseases, and even cellular regulation processes [47, 61].

Interest in INMT in psychiatry has grown in part due to its connection with the serotonin signaling pathway and specific receptors such as the sigma-1 receptor, which have been implicated in a variety of psychiatric disorders [47]. Further insights into the potential peripheral roles of INMT/DMT in mammalian systems, involving yet the sigma-1 receptor, are reported, especially in tissue protection, regeneration and immunity [24]. The colocalization of INMT with the sigma-1 receptor in primate spinal motor neurons suggests that it could be a target for treating schizophrenia and amyotrophic lateral sclerosis [31].

INMT exhibits widespread expression throughout the body, with high levels observed in lungs, thyroid, and adrenal gland. Intermediate levels are found in the placenta, skeletal muscle, heart, small intestine, stomach, pancreas, and lymph nodes. Moreover, INMT is densely localized at the anterior horn of the spinal cord [48, 65]. There is evidence that DMT is produced in the rat brain, with concentrations comparable to those of other monoamine neurotransmitters [20]. Additionally, the presence of INMT mRNA in various human brain regions, including the cerebral cortex, choroid plexus, and pineal gland is reported [20]. However, the exact function of INMT in biological systems remains uncertain at present. Nevertheless, numerous observations suggest the multifaceted significance of the *INMT* gene. For instance, researchers have revealed a decrease in the expression of the *INMT* gene in prostate cancer [40], lung cancer [38] and hepatocarcinoma [43], suggesting a potential role of INMT in inhibiting tumor progression.

To date, the activity of the human INMT (hINMT) has been described solely through radiometric assay with radiolabeled *S*-adenosylmethionine (SAM) to quantify the transfer of the methyl group from SAM to indole in the mono- and dimethylated products [68]. Alternatively, a chromatography-mass spectrometry approach has been employed to investigate the hINMT-catalyzed methylation of Tellurium compounds [64]. Therefore, no direct and continuous assays of this methyltransferase activity have been reported that can provide information on kinetic parameters and other biochemical characteristics of hINMT. Moreover, the existence of a single structure of hINMT in complex with *S*-adenosylhomocysteine (SAH), released over 20 years ago (PDB entry 2A14,

unpublished), highlights the significant gap in our understanding of this crucial yet underappreciated enzyme. Thus, unveiling the biochemical mechanisms and regulatory pathways of INMT, would offer valuable insights into the intricate interplay between neurotransmitter systems and brain function, with implications for both basic neurobiology and therapeutic interventions.

This study proposes an approach for the analysis of recombinant hINMT by elucidating its kinetic and structural characteristics. The core of the study is a noncoupled, continuous fluorescent assay, which has been yet employed to monitor the activity of a similar class I MT, nicotinamide N-methyltransferase (NNMT, EC 2.1.1.1) [51]. The fluorometric assay utilizes the substrate quinoline, which undergoes SAM-dependent hINMT-catalyzed methylation to produce 1-methylquinoline (1-MQ), exhibiting distinctive fluorescent properties that can be recorded using a standard spectrofluorometer. The assay is facilitated by straightforward thermal shift analysis employing a conventional PCR apparatus, which is well-known to assessing the stability of proteins [63] and determining affinity constants [54]. These analyses consistently yield thermal stability of hINMT under various conditions for the first time, as well as the dissociation constants associated with its natural coenzymes, SAM and SAH. Finally, open-access webservers are used to dock hINMT with quinoline (the assay substrate) or tryptamine (the natural substrate), to foresee the putative enzyme–substrate complexes and providing initial insights into the interactions, which further support the fluorometric dosage.

This approach serves as an alternative to the previously mentioned noncontinuous techniques, i.e., radiometric and chromatography-mass spectrometry assays. It offers functional and structural analysis under consistent conditions, which represents a novel contribution and would facilitate the investigation of hINMT SNPs, as well as the analysis of enzyme inhibition. Furthermore, the docking, guided by the known crystal structure of the hINMT-SAH complex (PDB code 2A14, unpublished), and the thermal shift data would enable the optimization of crystallization conditions to expand the limited structural information currently available.

Methods

cDNA cloning

The human *INMT* gene is 5471 base pairs long and consists of three exons. It shares structural similarities with the rabbit *INMT* gene, as well as with the genes encoding NNMT and phenylethanolamine N-methyltransferase (PNMT) across various species. All the exon–intron splice junctions in the *hINMT* gene followed the “GT-AG” rule, and there was no standard TATA or CAAT

sequences in the 5′-flanking region of the gene. Human *INMT* cDNA (isoform 1, Gene ID: 11,185) has a 792-bp open reading frame that encodes a 263-amino-acid protein. After codon optimization for the heterologous expression in *E. coli* bacterial cells, the hINMT cDNA sequence was synthesized and inserted into pET28b plasmid by 5′-NdeI and 3′-XhoI cloning sites. The resulting hINMT-pET28b vector was obtained from MWG Biotech (Eurofins Genomics).

Protein expression and purification

The hINMT enzyme was obtained through heterologous expression and purification, based on the procedure reported for hNNMT [51]. The hINMT-pET28b vector was transformed into competent *E. coli* BL21(DE3) pLysS cells (Novagen, Merck KGaA) via heat shock treatment, before plating on solid LB-Agar medium (Merck KGaA) containing kanamycin 30 µg/mL (Merck KGaA).

After overnight incubation at 37 °C, a single colony was selected and transferred into 20 mL of LB liquid medium containing kanamycin (Merck KGaA) and grown overnight at 37 °C with continuous shaking. The resulting cell suspension was then transferred into 1 L of fresh LB liquid medium supplemented with kanamycin, 0.5 mM MgCl₂, and 0.5 mM CaCl₂ (Merck KGaA). Cells were cultured until reaching an OD₆₀₀ of 0.7–0.8, at which point protein expression was induced by adding 0.5 mM isopropyl-β-D-1-thiogalactopyranoside (IPTG, Thermo Fisher Scientific, Inc.), followed by an additional 3-h incubation.

The culture was then centrifuged at 8 °C and 3000 rpm for 30 min to collect cells and resuspended in lysis buffer containing 20 mM TRIS-HCl pH 7.9 (Merck KGaA), 0.5 M NaCl (Merck KGaA), 5 mM imidazole (Merck KGaA), 10% glycerol (Merck KGaA), 1 mM dithiothreitol (DTT, Merck KGaA) and 1 mM phenylmethanesulfonyl-fluoride (PMSF, Thermo Fisher Scientific, Inc.).

After sonicating the sample at 30% amplitude with a pulse cycle of 3 s on and 9 s off to release the cytosolic content, while keeping the suspension on ice, debris and insoluble cell fractions were removed by centrifugation at 8 °C and 20,000 rpm for 45 min. The resulting soluble fraction was filtered through 0.45 µm filters (Merck KGaA) and loaded onto a 5 mL Sepharose affinity column (GE Healthcare), pre-treated with 100 mM NiSO₄ (Fisher Scientific) and equilibrated with a binding buffer: 20 mM TRIS-HCl (pH 7.9), 0.5 M NaCl, 5 mM imidazole, 10% glycerol, and 1 mM DTT. The protein was eluted using a gradient of elution buffer containing 500 mM imidazole at a flow rate of 2 mL/min, with fractions collected in small aliquots. The eluted fractions were analyzed by denaturing SDS-PAGE in 12% Mini-PROTEAN® TGX™ Precast Protein Gels (Bio-Rad Laboratories, Inc.)

alongside with a commercial PageRuler Plus Prestained Protein Ladder (Thermo Fisher Scientific, Inc.) and stained with a solution of Coomassie® Blu R 250 (Merck KGaA). The protein-containing fractions were enriched with 5 mM ethylenediaminetetraacetic acid (EDTA, Merck KGaA) to eliminate any eventual nickel ion etched by the protein, according to previous studies [5] and preserved at 8 °C for further use.

Protein quantification

The protein content was measured by UV–Vis spectrophotometry and bicinchoninic acid assay (BCA).

The former method involved a Cary-60 UV–VIS spectrophotometer (Agilent Technologies, Inc.) in a 1 cm quartz cuvette (Hellma GmbH & Co. KG). An extinction coefficient of 29,910 M⁻¹ cm⁻¹ and a protein molecular weight of 28.8 kDa were considered, as calculated using the ProtParam online tool from ExPASy (<https://web.expasy.org/protparam/>) [27].

The BCA-based quantification was carried out using the commercial colorimetric Pierce™ BCA Protein Assay Kit (Thermo Fisher Scientific, Inc.). Briefly, the process involved detecting the protein-dependent reduction of Cu⁺² to Cu⁺¹, which in turn forms a complex with bicinchoninic acid that absorbs light at 562 nm, proportionally to the protein concentration. Known amounts of bovine serum albumin have been used as reference samples. The absorbances were measured spectrophotometrically in triplicates.

Steady-state kinetic assays for hINMT activity

The enzymatic reactions were carried out at room temperature (30 °C) using a 50 mM HEPES buffer at pH 7.5, supplemented with 1 mM DTT. Freshly purified INMT enzyme was introduced to the reaction buffer at a final concentration of 3.8 μM.

To determine the Michaelis constant (K_M) for quinoline, initial reaction velocities were measured in separate reactions with quinoline (Merck KGaA) at various concentrations of 25, 100, 200, 400, 600, 800 and 2000 μM. These reactions were conducted at a fixed concentration of SAM (Merck KGaA) at 625 μM.

The K_M value for the co-substrate SAM was determined by measuring the initial reaction velocities varying SAM concentrations of 5, 25, 50, 100, 200, 400, 600, 800 and 2000 μM. These measurements were carried out with a fixed quinoline concentration of 800 μM.

The enzymatic reaction product 1-MQ was monitored by recording its fluorescence emission at 405 nm using a spectrofluorometer (Perkin Elmer LS 50 B), with an excitation wavelength λ_{ex} = 330 nm, according to the assay reported elsewhere for hNNMT [51]. The data were analyzed by KaleidaGraph v4.1 (Synergy Software). The

methylation of quinoline was monitored in the presence of varying amounts of tryptamine (200, 400, and 800 μM) added to the previously described reaction mixture.

Thermal shift assay (TSA)

The thermal stability of hINMT was evaluated by measuring its melting temperature (T_m) in response to pH, additives and ligands, as commonly reported [29, 33, 71, 55]. Each condition involved preparing 25 μL of sample in triplicate within dark-bottomed 96-well plates, sealing with transparent tape to prevent evaporation, briefly centrifuging to remove bubbles, and loading into a CFX Opus thermocycler (Bio-Rad Laboratories, Inc.).

In the first series of experiments, hINMT at concentration 2 μM was mixed with the fluorescent dye SYPRO Orange 5X (Merck KGaA) in 50 mM MES pH 6.0 (Merck KGaA), Bis-TRIS pH 6.5 (Merck KGaA), MOPS pH 7 (Merck KGaA), HEPES pH 7.5 (Merck KGaA), TRIS-Cl pH 8.0 (Merck KGaA) or Bicine pH 9.0 (Merck KGaA). After sealing and centrifugation, the plates were subjected to thermal treatment including 1 min pre-warming at 25 °C followed by a steady gradient 25–95 °C with 0.5 °C increments every 5 s. As the protein unfolded, the dye lit up because it was binding to the protein. The emission fluorescence at 570 nm was recorded as the unfolding process happened.

The second round of tests was carried out similarly after incorporating NaCl into the buffers at concentration 50, 100, 150 or 200 mM.

The third series of experiments were performed on samples mixed with SAM, SAH (Merck KGaA), tryptamine (Merck KGaA) or quinoline at concentrations 4, 8, 16, 32, 64, 128, 256, 512, 1024 or 2048 μM under the condition ensuring the utmost level of stability (maximum T_m) found in the previous assays. In these experiments, all the samples were also supplemented with 1 mM DTT to guarantee complete reduction of the protein, due to the high number of cysteines (12 out of 263 amino acids), according to the deposited sequence (PDB entry 2A14, unpublished).

TSA data analysis and K_d determination

The TSA data were analyzed with the CFX Maestro software (Bio-Rad Laboratories, Inc.) to generate fluorescence curves and their first derivatives for determining the average T_m from triplicates of each experimental condition. By exploring T_m changes regarding pH, additives and ligands, a better understanding of favorable conditions for hINMT and ligand interactions was gained, provided that a significant thermal shift was recorded, according to the sensitivity of the assay ($\Delta T \geq 1$ °C) [59]. The examination of T_m shifts based on varying ligand

concentrations also provided additional insights into the binding affinity.

To analyze the relationship between T_m and ligand concentration, KaleidaGraph v4.1 was utilized for nonlinear curve fitting, leading to the calculation of the K_d values. The curve fitting was based on the following hyperbolic Eq. 1 assuming a binding regime and one-site ligand binding conditions:

$$T = T_{in} + \Delta T \cdot [L]/[L] + K_d \quad (1)$$

where T_{in} is the starting T_m (no ligands added), ΔT is the utmost shift observed, $[L]$ is the ligand concentration and K_d is the dissociation constant for the hINMT-ligand complex. This approach is well-known to assess the binding between ligands or inhibitors with their targets [6, 12, 46, 55, 69].

Molecular docking

The docking study aimed to reveal the putative interactions between hINMT and tryptamine or quinoline. In this context, the 1.9 Å crystal structure of hINMT in complex with SAH (PDB entry 2A14, unpublished) was used as the starting template. The simulations were performed using the online integrative modeling server HADDOCK2.4 (<https://wenmr.science.uu.nl/haddock2.4>) [34] to support the thermal shift and kinetics data and provide initial hypotheses about how the substrates might bind to the enzyme.

Prior to docking, the hINMT-SAH PDB file was modified by removing water and ion molecules using UCSF ChimeraX v1.6.1 [49] and ensuring proper atom names, numbering as well as the presence of the target chain, as required by the server rules. The PDB files of tryptamine (PubChem CID 1150) and quinoline (PubChem CID 7047) were used as substrates, after verifying that they met the necessary server's requirements.

The amino acids Tyr20, Tyr24, Leu164, Cys168, Thr198, Tyr204 and Tyr242 were selected as active residues to generate ambiguous interaction restraints, and the relative solvent accessibility threshold was set to 8%, while allowing the server to automatically find passive residues.

The three-dimensional models generated after docking were visually inspected by UCSF ChimeraX v1.6.1, provided that their HADDOCK scores and z-scores were both negative.

Additional computing models were generated using the online tool protein–ligand interaction profiler (PLIP, <https://plip-tool.biotec.tu-dresden.de/plip-web/plip/index>) [2] to identify non-covalent interactions between hINMT and substrates, thus highlighting potential residues involved in the binding. For this purpose, the best models obtained by docking were used as entry

structures, without changing the default parameters provided by the server.

Results

The quinoline-based fluorescent method provides kinetics parameters for hINMT activity

Approximately 5 mg of purified hINMT was obtained per liter of bacterial culture. The specific activity of the enzyme was found to vary between 55.26 and 10 $\mu\text{moles per minute}^{-1} \text{ mg}^{-1}$ of enzyme, indicating a certain instability of the protein in solution, regardless of temperature (-20°C , 4°C) and/or different types of buffer solutions. The highest activity and best stability were obtained by dialyzing the protein immediately after chromatographic elution with 50 mM HEPES pH 7.5 supplemented with 50 mM NaCl and 1 mM DTT. The protein showed better stability when stored at 4°C in the same buffer supplemented with 1 mM DTT for a maximum of 48 h. Consistently, the Expasy ProtParam determined an instability index of 48.22 based on the protein amino acid sequence (PDB entry 2A14, unpublished), which classifies it as unstable.

As reported in the literature [51], NNMT is able to methylate quinoline via SAM, producing 1-MQ, which is fluorescent and thus allows for continuous monitoring of the activity. Alike, the same assay performed using the hINMT showed that the enzyme is also capable of methylating quinoline and the increase in fluorescence is stable over time and proportional to the amount of enzyme. These experiments allowed for the calculation of the catalytic parameters K_M and k_{cat} related to both quinoline and SAM under steady-state conditions using an enzyme concentration of 3.8 μM . Graphing the initial velocity for 1-MQ formation at different quinoline amounts (0–2000 μM) under fixed SAM concentration (625 μM) resulted in hyperbolic fitting according to a classical Michaelis–Menten trend (Fig. 1A). The calculated K_M value was $259.3 \pm 42.7 \mu\text{M}$. Similarly, steady-state runs at fixed quinoline concentration (800 μM), and variable SAM amounts (0–2000 μM) showed hyperbolic curves with calculated K_M of $64.1 \pm 3.9 \mu\text{M}$ (Fig. 1B). No changes in fluorescence were recorded in enzyme-free control experiments (data not shown). To note, the K_M related to SAM was comparable to the K_d ($55.6 \pm 2.6 \mu\text{M}$) measured by thermal shift assays (see below).

According to the measured V_{max} and enzyme concentration the values of the k_{cat} for quinoline resulted $3 \times 10^{-4} \text{ s}^{-1}$ and concerning SAM $7 \times 10^{-4} \text{ s}^{-1}$. Specificity constants, k_{cat}/K_M for quinoline and SAM resulted $1.15 \text{ s}^{-1} \cdot \text{M}^{-1}$ and $10.9 \text{ s}^{-1} \cdot \text{M}^{-1}$, respectively. The enzymatic activity of recombinant human INMT was measured at various temperatures (Figure S1) and pH values (Figure S2), showing that pH 7.5 and 37°C were optimal.

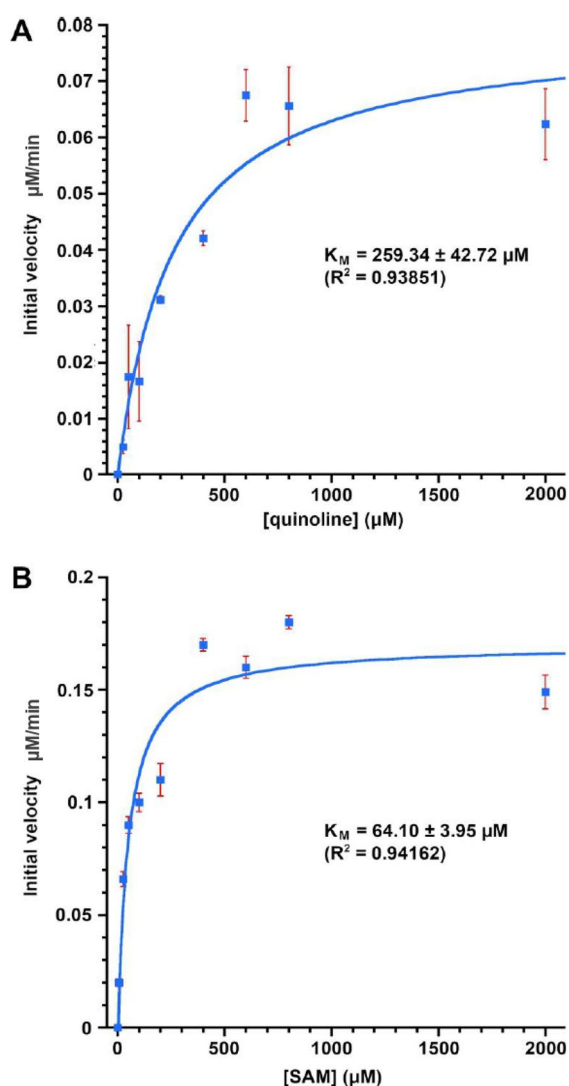


Fig. 1 Steady-state kinetics for SAM-dependent 1-MQ synthesis catalyzed by hINMT. The graphs report on the changes of initial velocity of 1-MQ formation when increasing amounts of **A** quinoline or **B** SAM are added to hINMT. The data have been fitted using the Michaelis–Menten equation to estimate the K_M values

The methylation of quinoline in the presence of varying amounts of the natural substrate tryptamine showed strong inhibition (Figure S3), as shown in Table 1, which reports on the residual activity of the hINMT enzyme in the formation of 1-MQ.

Further outcomes about the kinetic behavior of hINMT were obtained by testing the inhibitor activity of the molecule Naratriptan, which is known to hinder the MTs-catalyzed transmethylation reaction [66]. Steady-state experiments using the quinoline fluorometric method have emerged that Naratriptan inhibited conspicuously the hINMT activity with an estimated IC_{50} of $188.5 \pm 1.8 \mu\text{M}$.

Reducing, acid and neutral pH conditions stabilize hINMT

The thermal stability of hINMT was investigated by TSA, examining the effects of pH (6.0–9.0) and NaCl (0–200 mM). Though its small size (263 amino acids, MW=28.8 kDa), the protein exhibited two distinct T_m under all pH and saline conditions, as observed in the double peaks of the fluorescence derivative curves (Figure S4, T_{m1} and T_{m2}). For comparative analyses, the T_m associated with the first peak (T_{m1}) was considered the relevant data point.

In the absence of salt, the highest melting temperatures were observed between pH 6.0 and 7.0, with the latter providing the maximum stability, reaching $T_{m1} = 44.3 \pm 0.2 \text{ }^\circ\text{C}$. Conversely, the protein exhibited substantial instability at alkaline pH, with pH 9.0 causing the T_{m1} to drop to the minimum value of $39.2 \pm 0.8 \text{ }^\circ\text{C}$ (Figure S4A). Outside the pH range 6.0–9.0, the protein visibly began to precipitate (data not shown).

To note, the addition of NaCl led to a significant decrease in thermal stability, proportional to the salt concentration. The maximum T_{m1} was observed at pH 7.0 and 50 mM NaCl, reaching $T_{m1} = 43.7 \pm 0.2 \text{ }^\circ\text{C}$ and decreasing conspicuously to $34 \pm 0.4 \text{ }^\circ\text{C}$ at pH 9.0 and 200 mM NaCl (Figure S4B).

The data gathered from these experiments demonstrated that acidic and neutral environments favored the thermal stability of the enzyme. Conversely, alkaline

Table 1 Percentage of residual enzymatic activity of hINMT in methylating quinoline in the presence of tryptamine

Residual hINMT activity in the presence of tryptamine				
	100 μM quinoline	200 μM quinoline	400 μM quinoline	800 μM quinoline
0 μM tryptamine	100%	100%	100%	100%
200 μM tryptamine	80% \pm 16.5	65% \pm 10.8	81.2% \pm 2.15	85.2% \pm 5.65
400 μM tryptamine	51.6% \pm 1.75	52.2% \pm 13.95	63.4% \pm 9.3	78.8% \pm 8.4
800 μM tryptamine	12.9% \pm 1.95	27.8% \pm 0.25	47.6% \pm 10.45	44.8% \pm 0.45

Table 2 Average T_{m1} values of hINMT in response to pH and NaCl

	pH 6.0	pH 6.5	pH 7.0	pH 7.5	pH 8.0	pH 9.0
no NaCl	43.5 ± 0.2 °C	43.7 ± 0.2 °C	44.3 ± 0.2 °C	42.8 ± 0.2 °C	42 ± 0 °C	39.2 ± 0.8 °C
50 mM NaCl	43.3 ± 0.2 °C	43.5 ± 0 °C	43.7 ± 0.2 °C	42.3 ± 0.2 °C	41.2 ± 0.2 °C	37.3 ± 0.4 °C
100 mM NaCl	43.2 ± 0.2 °C	43.2 ± 0.2 °C	43 ± 0 °C	40.8 ± 0.6 °C	39.3 ± 0.2 °C	36.7 ± 0.8 °C
150 mM NaCl	42.8 ± 0.2 °C	43 ± 0.4 °C	42.5 ± 0 °C	40.2 ± 0.2 °C	39.3 ± 0.2 °C	35 ± 0.7 °C
200 mM NaCl	42.2 ± 0.2 °C	41.7 ± 0.9 °C	41 ± 0.4 °C	40.5 ± 0.7 °C	39.2 ± 0.5 °C	34 ± 0.4 °C

The T_m is determined at the first peak of each fluorescence derivative curve (T_{m1}) illustrated in Figure S4. The values are highlighted from green indicating the highest T_{m1} (maximum stability) to red representing the lowest value (minimum stability).

conditions and high salt concentrations caused substantial instability (Table 2).

To note, simultaneous inclusion of 1 mM DTT partially restored the T_{m1} by 0.5 °C on average even in the presence of NaCl across all tested pH values, with pH 7.0 still being optimal, giving a $T_{m1}=43.7\pm 0.2$ °C (data not shown), likely due to the reduction of the many cysteines present in hINMT. For this reason, to strike a balance between protein stability and maintaining the correct ionic strength and reducing environment, mimicking the cytoplasm, the next experiments were conducted at pH 7.5, with 50 mM sodium chloride and 1 mM DTT. This condition offered a fair balance satisfying both aspects and ensuring $T_{m1}=43.2\pm 0.4$ °C, still considered acceptable.

The double T_m detected over all experimental conditions could be related to the anticipated instability of hINMT, as computed by the ProtParam tool. Indeed, based on its amino acid sequence (PDB entry 2A14, unpublished), the instability index of hINMT is 48.22, which classifies it as unstable. Thus, there could be a heterogeneous population of molecules, each with distinct thermal stability. Alternatively, the denaturation process itself may cause multiple thermal transitions. This is often due to different structural domains responding separately to temperature changes [11, 19]. Supporting this hypothesis, it should be recalled that hINMT might possess several domains as observed in other similar enzymes, such as NNMT from humans, monkeys and mice (see below the structural description paragraph). Finally, the co-purification of hINMT along with host cells' endogenous

ligands could also result in a heterogeneous population of the enzyme. In fact, there is evidence that *E. coli*, engineered to express hINMT, can produce DMT without addition of SAM [25]. In such cases, proteins that exhibit a single T_m may show multiple thermal transitions upon ligand binding or vice versa [69], especially in the case of high-affinity binding events [44].

The destabilizing effect of alkaline pH and high NaCl concentrations on hINMT might be ascribed to its amino acids content and net charge. According to the ProtParam tool, in fact, the enzyme has a theoretical pI = 5.23, due to 40 acid residues (15 aspartates, 20 glutamates and 5 histidines) and 27 positively charged residues (17 lysines and 10 arginines). The acid pI puts hINMT within the large cluster of cytosolic human proteins [67]. Additionally, based on the Prot Pi online tool (<https://www.protpi.ch/Calculator/ProteinTool>), hINMT exhibits net negative charges of - 4.7 (pH 6.0), - 6.85 (pH 6.5), - 8.54 (pH 7.0), - 10.4 (pH 7.5), - 13.37 (pH 8.0) and - 22.53 (pH 9.0). The stability of a protein is primarily determined by the balance between repulsive forces between similar charges and attractive forces between opposite charges in its folded state. This delicate equilibrium, in fact, can be manipulated by modifying the surface charges of the protein, allowing for potential changes in its overall stability [3, 32]. Therefore, the instability of hINMT observed upon rising the pH would probably come from the repulsion among the many acid residues becoming more and more negatively charged. Furthermore, the steric hindrance may also play a role. Lysines are extended, flexible amino acids often found on the surface of proteins, where

they can readily interact with the surrounding solvent. This positioning allows them to be easily protonated at low pH, resulting in complete shielding of the positive charges by the solvent. In contrast, carboxyl residues, i.e., glutamates and aspartates, are generally less extended and more compact and this can lead to unfavorable structural effects when the charges on these residues become desolvated at high pH [41].

The stabilizing effect provided by DTT on hINMT is likely due to its role in preserving the reduced state of the twelve cysteine residues found in the amino acid sequence (PDB entry 2A14, unpublished; see below the structural description paragraph). Indeed, the structure shows all cysteines with reduced thiols, where the residues Cys44 and Cys254 as well as Cys168 and Cys213 lie close to each other (Sulphur-Sulphur distance = 4.3 and 4.2 Å, respectively). Moreover, it is reported that the reduction of the Cys44–Cys254 disulfide bond increases the catalysis of hINMT [68]. Though this assumption is speculative due to the poor availability of structural data, it is likely that DTT prevents covalent disulfide bridges that could destabilize the enzyme. Nevertheless, the diverse oxidation states of the numerous cysteines that might be still present could lead to a heterogeneous population. This, alongside the chance that the enzyme is composed of multiple distinct domains, might account for the two different melting temperatures.

SAM and SAH stabilize and bind to hINMT with micromolar affinity

After selecting the ideal setup to guarantee acceptable stability of hINMT while mimicking a native environment (pH 7.5, 50 mM NaCl, 1 mM DTT), additional TSA experiments were performed to get deeper into the effects of the coenzymes SAM and SAH as well as the substrates tryptamine and quinoline. The data showed that an increase in SAM concentration (0 to 2048 μM) led to a remarkable increase in T_{m1} , rising from 43.3 ± 0.2 °C (no SAM) to 50.5 ± 0 °C (2048 μM SAM), resulting in $\Delta T_{m1} = +7.2$ °C (Figure S5A). A similar trend was observed when assessing the effect of SAH, reaching $\Delta T_{m1} = +8.5$ °C (Figure S5B). To note, in this case the second T_m (T_{m2}) value was clearly absent.

On the other hand, both tryptamine and quinoline did not induce significant thermal transitions at any of the concentrations tested (0 to 2048 μM), giving $\Delta T_{m1} = 0.7$ °C and 0.8 °C, respectively (data not shown).

The remarkable positive temperature shifts induced by SAM and SAH (Table 3) made it possible to graph the changes of the T_{m1} values relative to the concentration of coenzymes. Fitting the curve based on a single-binding site and the hyperbolic Eq. 1 resulted

Table 3 Average T_{m1} values of hINMT in response to SAM and SAH

	SAM ($\Delta T_{m1} = +7.2$ °C)	SAH ($\Delta T_{m1} = +8.5$ °C)
0 μM	43.3 ± 0.2 °C	43.3 ± 0.2 °C
4 μM	44.3 ± 0.2 °C	44.3 ± 0.2 °C
8 μM	45.2 ± 0.2 °C	45.3 ± 0.2 °C
16 μM	46 ± 0 °C	46 ± 0 °C
32 μM	46.5 ± 0 °C	46.7 ± 0.2 °C
64 μM	47.3 ± 0.2 °C	47.3 ± 0.2 °C
128 μM	48 ± 0 °C	48.2 ± 0.2 °C
256 μM	49 ± 0 °C	49 ± 0 °C
512 μM	49.8 ± 0.2 °C	49.8 ± 0.2 °C
1024 μM	50.7 ± 0.2 °C	50.5 ± 0 °C
2048 μM	50.5 ± 0 °C	51.8 ± 0.2 °C

The T_m is determined at the first peak of each fluorescence derivative curve (T_{m1}) illustrated in Figure S5. The results related to tryptamine and quinoline are omitted due to no significant effects

in appropriate fitting and provided the estimation of K_d values of 55.6 ± 2.6 and 53.1 ± 4.8 μM, for SAM and SAH, respectively (Fig. 2). No K_d could be estimated for tryptamine and quinoline, likely because they are processed and released by the enzyme during turnover.

The T_{m1} shift caused by SAM and SAH indicates a stable interaction with the enzyme for it is consistent with other findings, showing that the binding of natural ligands to their targets typically has a measurable, stabilizing influence [6, 12, 46, 69]. This effect is due to thermodynamically favored binding that releases free energy ($\Delta G < 0$), pushing the protein–ligand complex into a lower, stable energy level [23, 52]. Therefore, when hINMT binds to coenzymes, it stabilizes in a way that requires higher temperatures to reach the melting point.

Nonetheless, the calculated K_d values (55.6 ± 2.6 and 53.1 ± 4.8 μM for SAM and SAH, respectively) were determined based on measures under in vitro conditions that most likely do not reflect the physiological environment. Therefore, these should be viewed as “apparent” values. Anyway, the order of magnitude (μM) is comparable with those determined elsewhere for other MTs [4, 14, 15, 51, 70]. Moreover, these values can be considered trustworthy as the TSA analyses have been performed using a protein concentration (2 μM) significantly lower than the calculated K_d , therefore satisfying a binding regime [35].

The kinetics and ligand affinity parameters related to substrates, coenzymes and the inhibitor reported in this paper are collected altogether for a more comprehensive understating of hINMT (Table 4).

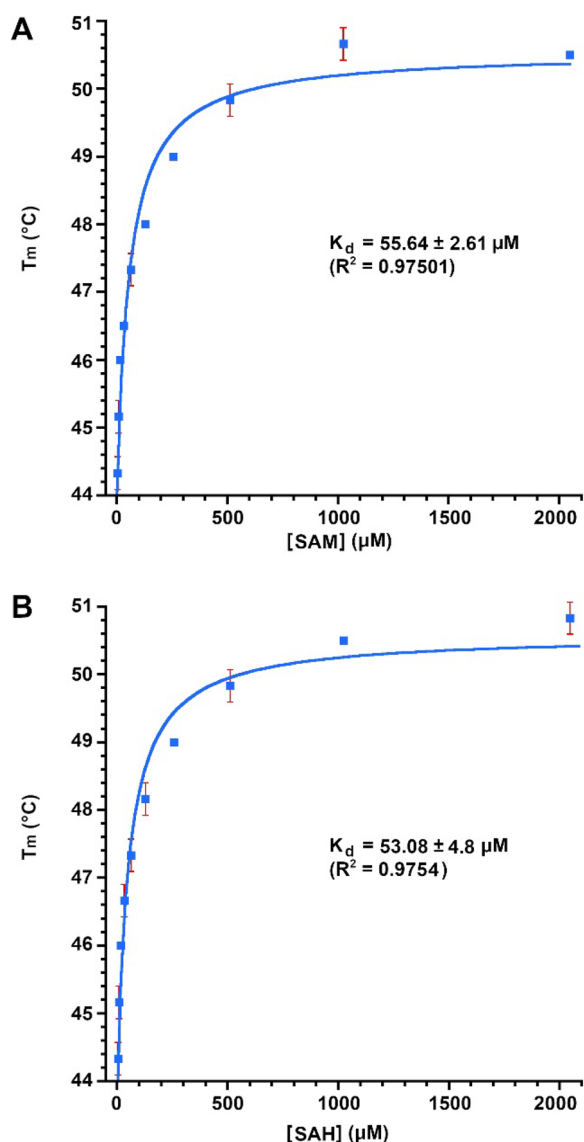


Fig. 2 T_{m1} shift in response to SAM or SAH, fitting and K_d estimation. The graphs depict the change in T_{m1} when increasing amounts of **A** SAM or **B** SAH are added, based on the information in Table 3. The data have been fitted using the hyperbolic, single-binding site Eq. 1 to estimate the K_d values

Structural description of hINMT: a comparison with similar MTs

The crystal structure of hINMT bound to SAH (PDB code 2A14, unpublished) is characterized by the Rossmann fold, a common feature of class I MTs. The cofactor attaches within an inner cavity surrounded by Ala169, Phe86, Val143, Ala165, Tyr204, Asp142, Asp85, Thr87, Leu163, Gly63, Tyr20, Tyr25 and Tyr69 (Fig. 3A). This area should also accommodate the substrate, tryptamine or quinoline, and the residues that it binds to, as suggested by the docking analysis reported herein (see below Fig. 4B). Since structural information on hINMT is limited to a single PDB entry, a comparison with paralogous enzymes, whose structure–function relationship is better characterized, could reveal interesting insights. The hINMT shares significant similarity with its close relative, hNNMT, with 67.4% sequence identity and 53% overall similarity [26] (see below Fig. 4C). hNNMT has been extensively studied, with 27 distinct PDB entries available. Notably, hNNMT features a region previously described as the “cap”, which is not present in the canonical Rossmann fold [53]. This structural element is also present in hINMT (Fig. 3B), thus representing an extra domain in MTs. Furthermore, other hINMT’s paralogs, like NNMTs found in monkeys and mice (PDB codes 5XVQ and 5XVK, respectively), have been shown to have three main parts: an N-terminal, a central, and a C-terminal domain [62]. Because of this, hINMT probably has those same three separate parts, along with the “cap”. Namely, the N-terminal, central and C-terminal domains in hINMT would correspond to residues in position 5 to 51, 52 to 189 and 190 to 261, respectively (Fig. 3B).

Finally, it is worth noting that the hINMT structure contains a high number of cysteines, with 12 out of 263 amino acids. Among these, the Sulphur atoms of Cys254 and Cys44 are separated by 4.3 Å, and a rotation around the α -C β bond could bring them within disulfide bond-forming distance (not shown). Similarly, Cys213 and Cys168, located near the active site, may also interact covalently in a comparable manner, given their Sulphur-Sulphur distance (4.2 Å). To note, both cysteine couples localize at the boundaries amongst domains. Specifically, Cys168 belongs to the central domain and Cys213 takes part of the C-terminal one, while Cys44 and Cys254 are

Table 4 Kinetics and ligand affinity parameters experimentally obtained in this paper

Ligand	K_d	K_M	k_{cat}	k_{cat}/K_M	IC_{50}
Quinoline	–	$259.3 \pm 42.7 \mu\text{M}$	$3 \times 10^{-4} \text{ s}^{-1}$	$1.15 \text{ s}^{-1} \text{ M}^{-1}$	–
SAM	$55.6 \pm 2.6 \mu\text{M}$	$64.1 \pm 3.9 \mu\text{M}$	$7 \times 10^{-4} \text{ s}^{-1}$	$10.93 \text{ s}^{-1} \text{ M}^{-1}$	–
SAH	$53.1 \pm 4.8 \mu\text{M}$	–	–	–	–
Naratriptan	–	–	–	–	$188.5 \pm 1.8 \mu\text{M}$

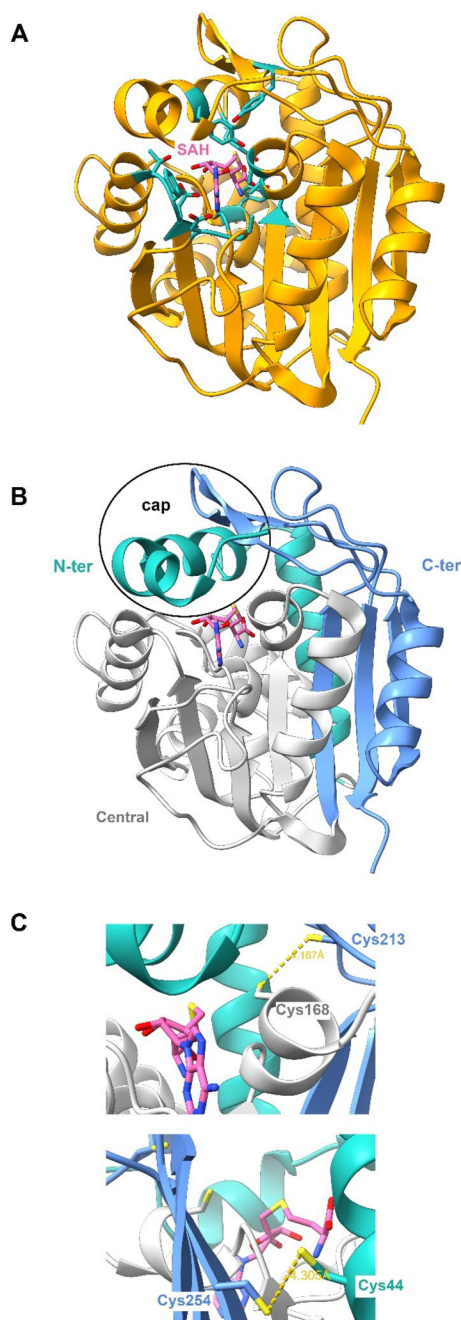


Fig. 3 Structural features of hINMT. **A** Structure overview of hINMT (PDB code 2A14, unpublished) showing the protein fold, the binding site of SAH (pink) and its ligands (in sticks). **B** The “cap”, N-terminal, central and C-terminal domains proposed for hINMT, based on the similarity to related proteins, i.e., NNMT from humans (PDB code 5YJF), mice (PDB code 5XVK) and monkeys (PDB code 5XVQ). **C** The four non-conserved cysteine residues in hINMT (in sticks). Due to their proximity, Cys213 and Cys168 probably create a disulfide bond. Alike, Cys254 and Cys44 can bind covalently

in the N-terminal and C-terminal domains, respectively (Fig. 3C). Though disulfide bonds are generally considered stabilizing, their location at domain boundaries may also allow for a degree of flexibility, enabling the domains to reorient themselves in response to ligand binding or other environmental changes. In this scenario, the disulfide bridges would not provide structural support but also contribute to the dynamic nature of hINMT, facilitating its interaction with other molecules and enabling it to carry out its biological function.

Tryptamine and quinoline share the same binding site in hINMT

The docking analyses have been carried out to get information about the putative positioning of tryptamine (the native substrate) or quinoline (the assay substrate) within the enzyme. The docking generated at least two acceptable models in both cases. The first model for the hINMT-SAH-tryptamine complex (HADDOCK score = -41.4 ± 1.2 , z-score = -1.6) showed the substrate located in a channel-like site bordered by the residues Phe5, Thr6, Asp8, Tyr11, Phe86, Asp142, Val143, His144, Cys168 and Ala169. Similarly, the first hINMT-SAH-quinoline model (HADDOCK score = -23.42 ± 1.3 , z-score = -1.5) also showed the compound in the same site (Fig. 4A).

The second docking models of the hINMT-SAH-tryptamine (HADDOCK score = -35.1 ± 1.7 ; z-score = -1) and hINMT-SAH-quinoline complex (HADDOCK score = -18.53 ± 1.9 ; z-score = -1.1) positioned both substrates within an inner cavity of the enzyme, near SAH. In this position, the substrates' amine acceptor was close to the coenzyme's Sulphur (Nitrogen-Sulphur distance = 4.1 \AA and 3.7 \AA for tryptamine and quinoline, respectively). Note that in SAM the Sulphur atom binds the methyl involved in transmethylation (Fig. 4B).

Supporting these results, structural alignments showed that the position of tryptamine and quinoline matched the site where two competitive inhibitors, i.e., 6-methoxynicotinamide and 5-cholorobenzoimidazole, have been found in the crystal structures of hNNMT-SAH (PDB entry 5YJF) [37] and hPNMT-SAH (PDB entry 3KQW) [22], also belonging to class I MTs (Fig. 4C).

A more detailed understanding of the interaction between quinoline or tryptamine and hINMT has been achieved by analyzing the amino acids surrounding the ligands when bound to the inner cavity of the enzyme using the protein–ligand interactions identifier PLIP [2]. The models showed several residues involved in these interactions, with hydrophobic bonds being the predominant type. Many of these residues were shared between

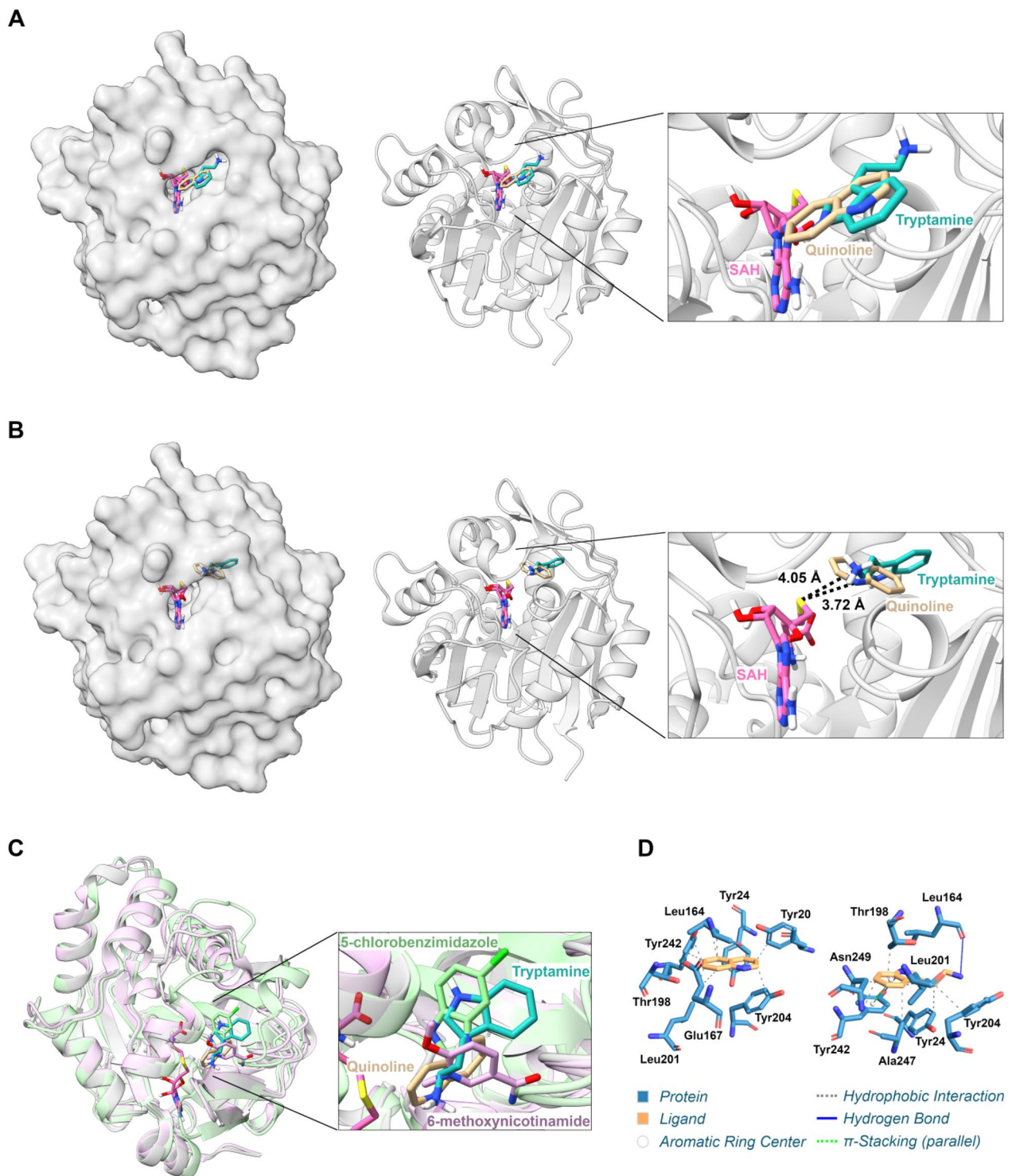


Fig. 4 Docking of hINMT-SAH with tryptamine or quinoline and putative interactions involved. **A** First and **B** second docking models of hINMT-SAH-tryptamine and hINMT-SAH-quinoline. The enzyme structure is shown as a continuous grey surface or ribbons; the two substrates and the coenzyme are represented as colored sticks. Models were generated using the HADDOCK webservice. **C** Superposition of the second hINMT-SAH-tryptamine and hINMT-SAH-quinoline models (grey) with the crystal structures of hINMT-SAH (pink) and hPNMT-SAH (green) bound to competitive inhibitors. Images visualized using ChimeraX. **D** Putative residues at the active site involved in the interactions between hINMT and quinoline (left) or tryptamine (right). Models were generated by the PLIP webservice

remains an assumption without direct experimental evidence to support the claim.

Discussion

DMT and INMT are attracting growing interest, especially within the emerging “psychedelic renaissance” [13, 28]. Hence, the need for trustworthy, straightforward approaches to explore the role of DMT and INMT became significant.

DMT is found ubiquitously in plants and animals, with its presence detected in the cerebrospinal fluid and brain of the latter. Its levels fluctuate throughout the day and with age and even increase during times of stress [36]. INMT appears even more complicated. This enzyme is found in many different organs including brain, lungs, kidneys, heart, retina, and the testes, among many others [36]. Furthermore, though numerous single SNPs in the *INMT* gene are associated with various behavioral traits and medical conditions, yet little research has explored how these genetic differences relate to the synthesis of DMT [21]. Moreover, only one structure, related to the hINMT-SAH complex and released now 20 years ago, is available so far (PDB entry 2A14, unpublished), limiting the information about the structure–function relationships in hINMT mutants.

In such a captivating but still challenging scenario, this paper aimed to provide a route for studying hINMT under consistent conditions, without the need for derivatization or extrapolation of the enzymatic reaction product. This is significant, as past research on the enzymatic activity of hINMT has revealed substantial variations in the enzyme’s kinetic parameters, such as the K_M for its natural substrate, tryptamine. This parameter, indeed, was quantified in a wide range (430–2290 μM), using indirect methods like radioactive assays [17, 45, 65] or gas chromatography-mass spectrometry [56].

The TSA results reported in this paper represent one major improvement over previous studies. In fact, the kinetics assays presented in the afore-mentioned studies employing recombinant hINMT [17, 65] were carried out under alkaline conditions (8.5), while others used tissue extract [45, 56], which could suffer of poor reliability. In any case, the TSA clearly demonstrated that pH levels above 7.5 significantly reduce the enzyme’s stability (Figure S4 and Table 2) and potentially hinder the kinetic measurements. Consequently, the accuracy of the K_M values published until now may be questioned.

Moreover, finding the right conditions *in vitro* by TSA would assist in discovering suitable conditions for future structural studies, e.g., screening of hINMT SNPs, using a common PCR device. It must be recalled, indeed, that hINMT is inherently unstable for its amino acid

composition, regardless of the conditions used (instability index = 48.22, see above).

The findings from the TSA also provided insights into the coenzymes’ affinities for hINMT. The K_d values for both SAM and SAH are determined for the first time (Fig. 2). While these must be considered “apparent” values, they are consistent with the parameters observed for other MTs from different organisms [4, 14, 15, 51, 70]. This information can provide valuable insights for future structural analysis, potentially assisting in the development of new protein-coenzyme-inhibitor complexes for practical applications. However, the evident resemblance between the K_d of SAM and SAH raises a question. SAH should easily detach from the enzyme to facilitate the turnover, a process that would be hindered if the coenzymes exhibit similar affinities. To explain this result, one might speculate that the affinity of SAM for hINMT considerably improves in the presence of the substrate. As an example, it is reported that SAM undergoes up to 20-fold affinity increase for hNNMT when the enzyme is pre-bound to quinoline [51]. Given the high sequence identity (67.4%) and similarity (53%) between hINMT and hNNMT [64], it is likely that this may occur in hINMT as well. Moreover, the plasma and intracellular SAM concentrations are usually higher than SAH [60]. Thus, the binding of the substrate likely displaces the water molecules found experimentally in the active site (Figure S6). This increases the hydrophobicity of the site, allowing the methyl group of SAM to properly orient itself. Therefore, under normal physiological conditions, SAM may bind more strongly to hINMT than SAH, potentially facilitating the turnover process.

In previous studies, kinetic parameters of hINMT from other animal species either recombinant or purified from tissues, were calculated using a non-continuous assay with radioactive SAM. The K_M value of hINMT for the natural substrate tryptamine resulted 0.93–1.64 mM depending on experimental conditions [68]. Other authors have measured the kinetic parameters of INMT from different species, showing a K_M of $499 \pm 68 \mu\text{M}$ for the enzyme from rabbit lung [18] and 122 μM in *Bufo gargarizans* [72]. The extreme variability reflects the differences across animal species regarding the function of the produced amines but also the low reproducibility of a non-continuous assay with measurement of products separated using extraction or chromatographic techniques. In fact, K_M values for tryptamine were highly variable and in the micromolar range, indicating low affinity of the methyltransferase for its natural substrate.

Bar-Even et al. analyzed the k_{cat} and K_M values of several thousand enzymes collected from the literature. They identified that the “average enzyme” has a k_{cat} of approximately $\sim 10 \text{ s}^{-1}$ and a k_{cat}/K_M ratio of around

$10^{-5} \text{ s}^{-1} \text{ M}^{-1}$, well below the diffusion limit and what is typically reported in textbooks [7]. Moreover, the physicochemical properties of substrates influence kinetic parameters; specifically, low molecular mass and hydrophobicity appear to limit the optimization of K_M . Furthermore, tryptamine is enzymatically dimethylated and might exhibit different kinetic parameters if tested with an unmethylated or monomethylated substrate (mono-methyl-tryptamine).

The results obtained in this paper with hINMT using quinoline transformed into a monomethylated product (1-MQ) indicate a low affinity of the enzyme for quinoline ($K_M = 259.3 \pm 42.7 \mu\text{M}$). The K_M value for SAM is $64.10 \pm 3.95 \mu\text{M}$ indicating a higher affinity of the enzyme for its natural co-substrate.

The K_M value for quinoline was about 40% lower than the value measured for the enzyme NNMT, while the K_M value for SAM was approximately twice that of NNMT [51]. These data are consistent with the fact that, although the two enzymes belong to the same family of SAM-dependent MTs, they have different roles and specificity. The k_{cat} values for both quinoline and SAM resulted in the order of 10^{-4} s^{-1} . Similarly, Neelakantan et al. reported a comparably low value for hNNMT [51]. This data indicates that the catalysis is inefficient and that the rate-limiting step of the reaction may be particularly slow. Consequently, values of k_{cat}/K_M known as the specificity constant, resulted in a range of 1–10, far respect to the value of the “average enzyme”, indicating how slowly the enzyme can convert the substrates into the product when they are at low concentrations. A low efficiency regarding an artificial substrate is expected, while for the SAM substrate, it could indicate that the “in vivo” reaction is regulated by other factors.

The effect of tryptamine on the enzymatic activity of hINMT, monitored using the artificial substrate quinoline, is inhibitory. As the concentration of tryptamine increases, the inhibition also increases (Table 1). Namely, preliminary data have shown competitive inhibition (Figure S3), as expected, confirming that tryptamine and quinoline share the same binding site, as observed by docking analysis (Fig. 4B).

Finally, it must be noted that the IC_{50} of Naratriptan ($188.5 \pm 1.8 \mu\text{M}$) estimated by the quinoline-based fluorometric on hINMT method is highly consistent with previous results related to the rabbit INMT ($\text{IC}_{50} = 167 \mu\text{M}$) [66].

The lack of exhaustive structural data on hINMT, currently available as a single crystal structure in complex with SAH (PDB entry 2A14, unpublished), is likely the most significant obstacle in a comprehensive understanding of some of the enzyme SNPs, described in literature [21, 68]. However, the preliminary structure–function

analysis presented in this study provides valuable insights that may guide future investigations.

The existence of four domains in hINMT (the “cap”, N-terminal, central and C-terminal domain), obtained by comparative analysis with similar paralogs (Fig. 3), might explain the double transition observed during TSA (Figure S4).

Besides this, one should also consider the presence of two couple of cysteines residues, i.e., Cys213–Cys168 and Cys44–Cys254, that localize at the boundaries of these domains. These cysteine couples are in a reduced state but close enough to potentially form two disulfide bridges (Fig. 3C). It was mentioned that the addition of 1 mM DTT increases the thermal stability of hINMT by $0.5 \text{ }^\circ\text{C}$ on average, likely due to an increased reduction of these cysteine couples (see above TSA results). While cysteines are typically associated with stabilization of the structure, a significant body of evidence suggests that cleavable disulfide bonds can modulate protein allostery, leading to the concept of “allosteric” disulfides [16]. An example can be found in cyclophilin A from *Schistosoma mansoni*, whose reduced cysteines triggers the isomerase activity while oxidation turns it off [30]. Interestingly, none of the four cysteines found in hINMT are conserved in its close paralogs, such as NNMT from humans, mice, and monkeys. Moreover, among the various hINMT SNPs, the Cys254Phe variant retains enzymatic activity even in the absence of reducing conditions [68], suggesting a potential physiological and redox role for these non-conserved cysteine residues, which warrants further investigation in future studies.

The docking analysis showed a channel-like site (Fig. 4A), highlighted for the first time, as well as the high degree of conservation of the amino acids lining it amongst hINMT and its paralogs hNNMT and hPNMT, all belonging to class I MTs (Fig. 5, residues highlighted in yellow). This suggests that the channel might have a functional role, potentially serving as an entry and/or exit route for tryptamine and quinoline. However, this hypothesis would diverge from the one put forward elsewhere by molecular dynamics simulations, which presumes the existence of another channel responsible for the incorporation of substrates or the release of products [26].

The docking models also revealed for the first time the putative binding site of tryptamine in hINMT, which matches with the position of quinoline (Fig. 4B). It is worth nothing that the same residues also take part in binding to dimethylselenide (DMSe), a metabolite produced during the detoxification of Selenium excess, as shown elsewhere by molecular dynamics simulations [26]. Moreover, competitive inhibitors experimentally found in hNNMT (PDB entry 5YJF) [37] and hPNMT

(PDB entry 3KQW) [22], both in complex with SAH, occupy the same position (Fig. 4C), thus supporting the docking results. The highly conserved amino acids that make up the putative residues involved in binding tryptamine and quinoline in hINMT (Fig. 4D) further validate the docking models as they are highly conserved amongst the three MTs (Fig. 5, residues highlighted in green).

Conclusions

This research advances the understanding of the structural–functional relationships of hINMT by incorporating a novel continuous enzymatic assay, thermal shift experiments to determine the dissociation constants of SAM and SAH, and *in silico* bioinformatics analyses, including docking studies, structural, and sequence alignments, which support the use of quinoline as a model substrate for steady-state characterization. This advancement is particularly significant compared to previous assays, as it allows for more precise and continuous monitoring of enzymatic activity, which is essential for capturing subtle kinetic differences. In short, the assay of the hINMT enzyme using the artificial substrate quinoline has provided key kinetic properties that until now had resulted in variable outcomes and lengthy procedures.

The type of assay presented in this work is suitable for studying the activities and kinetics of protein mutants, analyzing specificities and active site characteristics, and testing potential inhibitors. Combined with the ability to determine dissociation constants through a straightforward method like TSA, this opens new avenues for investigating how polymorphisms may influence enzyme function—an area that remains largely unexplored. Consequently, it may provide deeper insights into the molecular basis of psychiatric diseases linked to genetic variations in hINMT. By connecting structural and functional alterations to disease phenotypes, this research lays the groundwork for developing targeted therapeutic interventions and offers a more comprehensive understanding of enzyme behavior and its role in pathology.

Abbreviations

MDMA	3,4-Methylenedioxymethamphetamine
MT	Methyltransferase
–CH ₃	Methyl group
SAM	S-adenosylmethionine
INMT	Indolethylamine <i>N</i> -methyltransferase
NMT	<i>N</i> -Methyltryptamine
DMT	<i>N,N</i> -Dimethyltryptamine
NMS	<i>N</i> -Methylserotonin
AADC	Aromatic-L-amino acid decarboxylase
SNPs	Single nucleotide polymorphisms
NNMT	Nicotinamide <i>N</i> -methyltransferase
1-MQ	1-Methylquinoline
SAH	S-adenosylhomocysteine
PNMT	Phenylethanolamine <i>N</i> -methyltransferase
IPTG	Isopropyl-β-D-1-thiogalactopyranoside

DTT	Dithiothreitol
EDTA	Ethylenediaminetetraacetic acid
BCA	Bicinchoninic acid assay
TSA	Thermal shift assay
T _m	Melting temperature
PLIP	Protein–ligand interaction profiler
S _N 2	Bimolecular nucleophilic substitution
DMSe	Dimethylselenide

Supplementary Information

The online version contains supplementary material available at <https://doi.org/10.1186/s13062-025-00632-z>.

Additional file 1.

Acknowledgements

Not applicable.

Author contributions

Conceptualization: F.A., R.I. and G.P.; methodology and investigation: F.R., L.P., F.G., M.P. and L.D.L.; data analysis: M.A. and F.A.; writing—original draft: M.A. and G.P.; writing—review & editing: F.A. and R.I.; supervision: M.A., R.I. and G.P.; funding acquisition: M.A., F.A. and R.I. All authors have reviewed the manuscript, approved the submitted version and agreed both to be personally accountable for the author's own contributions and to ensure that questions related to the accuracy or integrity of any part of the work, even ones in which the author was not personally involved, are appropriately investigated, resolved, and the resolution documented in the literature.

Funding

The study was supported by the “Vitality” PNRR program, funded by the European Commission (EU) (E13C22001060006), awarded to F.A. and R.I., and by “Progetti di Ateneo” 2022 and 2023 of the University of L'Aquila, granted to M.A. M.P. contributed to this publication while attending the PhD programme in PhD in Sustainable Development And Climate Change at the University School for Advanced Studies IUSS Pavia, Cycle XXXVIII, with the support of a scholarship financed by the Ministerial Decree no. 351 of 9th April 2022, based on the NRRP—funded by the European Union—NextGenerationEU—Mission 4 “Education and Research”, Component 1 “Enhancement of the offer of educational services: from nurseries to universities”—Investment 4.1 “Extension of the number of research doctorates and innovative doctorates for public administration and cultural heritage”. L.P. contributed to this publication while attending the PhD programme in PhD in Sustainable Development And Climate Change at the University School for Advanced Studies IUSS Pavia, Cycle XL, with the support of a scholarship co-financed by the Ministerial Decree no. 630/2024, based on the NRRP—funded by the European Union—NextGenerationEU—Mission 4 “Education and Research”, Component 2 “From Research to Business”, Investment 3.3, and by the company Dompé spa.

Availability of data and materials

No datasets were generated or analysed during the current study.

Declarations

Ethics approval and consent to participate

Not applicable.

Consent for publication

Not applicable.

Competing interests

The authors declare no competing interests.

Author details

¹Department of Life, Health and Environmental Sciences, University of L'Aquila, L'Aquila, Italy. ²Department of Science, Technology and Society, University School for Advanced Studies of Pavia, Pavia, Italy.

Received: 20 January 2025 Accepted: 13 March 2025
Published online: 10 April 2025

References

- Abdelraheem E, Thair B, Varela RF, Jockmann E, Popadić D, Hailes HC, Ward JM, Iribarren AM, Lewkowicz ES, Andexer JN, Hagedoorn PL, Hanefeld U. Methyltransferases functions and applications. *ChemBioChem*. 2022;23(18):202200212. <https://doi.org/10.1002/cbic.202200212>. (Epub 2022 Jul 5. PMID: 35691829; PMCID: PMC9539859).
- Adasme MF, Linnemann KL, Bolz SN, Kaiser F, Salentin S, Haupt VJ, Schroeder M. PLIP 2021: expanding the scope of the protein-ligand interaction profiler to DNA and RNA. *Nucleic Acids Res*. 2021;49:W530–4. <https://doi.org/10.1093/nar/gkab294>. (PMID:33950214;PMCID: PMC8262720).
- Akke M, Forsén S. Protein stability and electrostatic interactions between solvent exposed charged side chains. *Proteins*. 1990;8:23–9. <https://doi.org/10.1002/prot.340080106>. (PMID: 2217161).
- Aktas M, Gleichenhagen J, Stoll R, Narberhaus F. S-adenosylmethionine-binding properties of a bacterial phospholipid N-methyltransferase. *J Bacteriol*. 2011;193:3473–81. <https://doi.org/10.1128/JB.01539-10>.
- Ardini M, Huang JA, Caprettini V, De Angelis F, Fata F, Silvestri I, Cimini A, Giansanti F, Angelucci F, Ippoliti R. A ring-shaped protein clusters gold nanoparticles acting as molecular scaffold for plasmonic surfaces. *Biochim Biophys Acta Gen Subj*. 2020;1864: 129617. <https://doi.org/10.1016/j.bbagen.2020.129617>. (Epub 2020 Apr 15 PMID: 32304715).
- Bai N, Roder H, Dickson A, Karanickolas J. Isothermal analysis of ThermoFluor data can readily provide quantitative binding affinities. *Sci Rep*. 2019;9:2650. <https://doi.org/10.1038/s41598-018-37072-x>. PMID:30804351;PMCID:PMC6389909.
- Bar-Even A, Noor E, Savir Y, Liebermeister W, Davidi D, Tawfik DS, Milo R. The moderately efficient enzyme: evolutionary and physicochemical trends shaping enzyme parameters. *Biochemistry*. 2011;50(21):4402–10. <https://doi.org/10.1021/bi2002289>. (Epub 2011 May 4 PMID: 21506553).
- Barker SA, McIlhenny EH, Strassman R. A critical review of reports of endogenous psychedelic N, N-dimethyltryptamines in humans: 1955–2010. *Drug Test Anal*. 2012;4:617–35. <https://doi.org/10.1002/dta.422>. (Epub 2012 Feb 28 PMID: 22371425).
- Barker SA, Monti JA, Christian ST. N, N-dimethyltryptamine: an endogenous hallucinogen. *Int Rev Neurobiol*. 1981;22:83–110. [https://doi.org/10.1016/s0074-7742\(08\)60291-3](https://doi.org/10.1016/s0074-7742(08)60291-3). (PMID: 6792104).
- Barker SA. N, N-Dimethyltryptamine (DMT), an endogenous hallucinogen: past, present, and future research to determine its role and function. *Front Neurosci*. 2018;12:536. <https://doi.org/10.3389/fnins.2018.00536>. (PMID:30127713;PMCID:PMC6088236).
- Barroca-Ferreira J, Cruz-Vicente P, Santos MFA, Rocha SM, Santos-Silva T, Maia CJ, Passarinha LA. Enhanced stability of detergent-free human native STEAP1 protein from neoplastic prostate cancer cells upon an innovative isolation procedure. *Int J Mol Sci*. 2021;22:10012. <https://doi.org/10.3390/ijms221810012>. (PMID:34576175;PMCID:PMC8472055).
- Bhayani JA, Ballicora MA. Determination of dissociation constants of protein ligands by thermal shift assay. *Biochem Biophys Res Commun*. 2022;590:1–6. <https://doi.org/10.1016/j.bbrc.2021.12.041>. (Epub 2021 Dec 17 PMID: 34959191).
- Cameron LP, Olson DE. Dark classics in chemical neuroscience: N, N-dimethyltryptamine (DMT). *ACS Chem Neurosci*. 2018;9(10):2344–57. <https://doi.org/10.1021/acscchemneuro.8b00101>. (Epub 2018 Jul 23 PMID: 30036036).
- Chatterjee D, Kudlinzki D, Linhard V, Saxena K, Schieborr U, Gande SL, Wurm JP, Wöhnert J, Abele R, Rogov VV, Dötsch V, Osiewacz HD, Sreeramulu S, Schwalbe H. Structure and biophysical characterization of the S-adenosylmethionine-dependent O-methyltransferase PaMTH1, a putative enzyme accumulating during senescence of *Podospora anserina*. *J Biol Chem*. 2015;290:16415–30. <https://doi.org/10.1074/jbc.M115.660829>. (Epub 2015 May 15. PMID: 25979334; PMCID: PMC4481238).
- Chen H, Lin S, Yang F, Chen Z, Guo L, Yang J, Lin X, Wang L, Duan Y, Wen A, Zhang X, Dai Y, Yin K, Yuan X, Yu C, He Y, He B, Cao Y, Dong H, Li J, Zhao Q, Liu Q, Lu G. Structural and functional basis of low-affinity SAM/SAH-binding in the conserved MTase of the multi-segmented Alongshan virus distantly related to canonical unsegmented flaviviruses. *PLoS Pathog*. 2023;19: e1011694. <https://doi.org/10.1371/journal.ppat.1011694>. (PMID:37831643;PMCID:PMC10575543).
- Chiu J, Hogg PJ. Allosteric disulfides: sophisticated molecular structures enabling flexible protein regulation. *J Biol Chem*. 2019;294(8):2949–60. <https://doi.org/10.1074/jbc.REV118.005604>.
- Chu U, Mavlyutov T, Schulman A, Baker E, Raj R, Epstein M, Guo L, Ruoho A. Methylation of thiols and thioethers by human indolethylamine-N-methyl transferase. *FASEB J*. 2015;29:10227. https://doi.org/10.1096/fasebj.29.1_supplement.10227.
- Chu UB, Vorperian SK, Satyshur K, Eickstaedt K, Cozzi NV, Mavlyutov T, Hajipour AR, Ruoho AE. Noncompetitive inhibition of indolethylamine-N-methyltransferase by N, N-dimethyltryptamine and N, N-dimethylaminopropyltryptamine. *Biochemistry*. 2014;53(18):2956–65. <https://doi.org/10.1021/bi500175p>. (Epub 2014 Apr 28. PMID: 24730580; PMCID: PMC4025572).
- Dashivets T, Thomann M, Rueger P, Knaupp A, Buchner J, Schlothauer T. Multi-angle effector function analysis of human monoclonal IgG glyco-variants. *PLoS ONE*. 2015;10: e0143520. <https://doi.org/10.1371/journal.pone.0143520>. (PMID:26657484;PMCID:PMC4676693).
- Dean JG, Liu T, Huff S, Sheler B, Barker SA, Strassman RJ, Wang MM, Borjigin J. Biosynthesis and extracellular concentrations of N, N-dimethyltryptamine (DMT) in mammalian brain. *Sci Rep*. 2019;9:9333. <https://doi.org/10.1038/s41598-019-45812-w>. (PMID:31249368;PMCID: PMC6597727).
- Dean JG. Indolethylamine-N-methyltransferase Polymorphisms: genetic and biochemical approaches for study of endogenous N, N-dimethyltryptamine. *Front Neurosci*. 2018;12:232. <https://doi.org/10.3389/fnins.2018.00232>. (PMID:29740267;PMCID:PMC5924808).
- Drinkwater N, Vu H, Lovell KM, Criscione KR, Collins BM, Prinszano TE, Poulsen SA, McLeish MJ, Grunewald GL, Martin JL. Fragment-based screening by X-ray crystallography, MS and isothermal titration calorimetry to identify PNMT (phenylethanolamine N-methyltransferase) inhibitors. *Biochem J*. 2010;431:51–61. <https://doi.org/10.1042/BJ20100651>. (PMID: 20642456).
- Du X, Li Y, Xia YL, Ai SM, Liang J, Sang P, Ji XL, Liu SQ. Insights into protein-ligand interactions: mechanisms, models, and methods. *Int J Mol Sci*. 2016;17:144. <https://doi.org/10.3390/ijms17020144>. (PMID:26821017;PMCID:PMC4783878).
- Frecska E, Szabo A, Winkelmann MJ, Luna LE, McKenna DJ. A possibly sigma-1 receptor mediated role of dimethyltryptamine in tissue protection, regeneration, and immunity. *J Neural Transm*. 2013;120:1295–303. <https://doi.org/10.1007/s00702-013-1024-y>. (Epub 2013 Apr 26 PMID: 23619992).
- Friedberg LM, Sen AK, Nguyen Q, Tonucci GP, Hellwarth EB, Gibbons WJ Jr, Jones JA. In vivo biosynthesis of N, N-dimethyltryptamine, 5-MeO-N, N-dimethyltryptamine, and bufotenine in *E. coli*. *Metab Eng*. 2023;78:61–71. <https://doi.org/10.1016/j.ymben.2023.05.006>. (Epub 2023 May 23. PMID: 37230161).
- Fukumoto Y, Kyono R, Shibukawa Y, Tanaka YK, Suzuki N, Ogra Y. Differential molecular mechanisms of substrate recognition by selenium methyltransferases, INMT and TPMT, in selenium detoxification and excretion. *J Biol Chem*. 2023;300:105599. <https://doi.org/10.1016/j.jbc.2023.105599>. (Epub 2023 Dec 28. PMID: 38159853; PMCID: PMC10844679).
- Gasteiger E, Hoogland C, Gattiker A, Duvaud S, Wilkins MR, Appel RD, Bairoch A. Protein identification and analysis tools on the expasy server; (In) John M. Walker (ed): The Proteomics Protocols Handbook, Humana Press (2005). pp. 571–607. PMID: 10027275.
- George DR, Hanson R, Wilkinson D, et al. Ancient roots of today's emerging renaissance in psychedelic medicine. *Cult Med Psychiatry*. 2022;46:890–903. <https://doi.org/10.1007/s11013-021-09749-y>. (Epub 2021 Sep 2. PMID: 34476719; PMCID: PMC8412860).
- Gooran N, Kopra K. Fluorescence-based protein stability monitoring—a review. *Int J Mol Sci*. 2024;25:1764. <https://doi.org/10.3390/ijms25031764>. (PMID:38339045;PMCID:PMC10855643).
- Gourlay LJ, Angelucci F, Baiocco P, Boumris G, Brunori M, Bellelli A, Miele AE. The three-dimensional structure of two redox states of cyclophilin A from *Schistosoma mansoni*. Evidence for redox regulation of peptidyl-prolyl cis-trans isomerase activity. *J Biol Chem*.

- 2007;282(34):24851–34857. <https://doi.org/10.1074/jbc.M702714200>. (Epub 2007 Jun 25. PMID: 17591771).
31. Grammenos D, Barker SA. On the transmethylation hypothesis: stress, N, N-dimethyltryptamine, and positive symptoms of psychosis. *J Neural Transm (Vienna)*. 2015;122:733–9. <https://doi.org/10.1007/s00702-014-1329-5>. (Epub 2014 Nov 2. PMID: 25362533).
 32. Grimsley GR, Shaw KL, Fee LR, Alston RW, Huyghues-Despointes BM, Thurkill RL, Scholtz JM, Pace CN. Increasing protein stability by altering long-range coulombic interactions. *Protein Sci*. 1999;8:1843–9. <https://doi.org/10.1110/ps.8.9.1843>. (PMID:10493585;PMCID:PMC2144408).
 33. Grøftehaug MK, Hajizadeh NR, Swann MJ, Pohl E. Protein-ligand interactions investigated by thermal shift assays (TSA) and dual polarization interferometry (DPI). *Acta Crystallogr D Biol Crystallogr*. 2015;71:36–44. <https://doi.org/10.1107/S1399004714016617>. (Epub 2015 Jan 1. PMID: 25615858; PMCID: PMC4304684).
 34. Honorato RV, Trellet ME, Jiménez-García B, Schaarschmidt JJ, Giulini M, Reys V, Koukos PI, Rodrigues JPGLM, Karaca E, van Zundert GCP, Roel-Touris J, van Noort CW, Jandová Z, Melquiond ASJ, Bonvin AMJJ. The HADDOCK2.4 web server for integrative modeling of biomolecular complexes. *Nat Protoc*. 2024;19(11):3219–41. <https://doi.org/10.1038/s41596-024-01011-0>. (Epub 2024 Jun 17. PMID: 38886530).
 35. Jarmoskaite I, AlSadhan I, Vaidyanathan PP, Herschlag D. How to measure and evaluate binding affinities. *Elife*. 2020;9: e57264. <https://doi.org/10.7554/eLife.57264>. (PMID:32758356;PMCID:PMC7452723).
 36. Jiménez JH, Bouso JC. Significance of mammalian N, N-dimethyltryptamine (DMT): a 60-year-old debate. *J Psychopharmacol*. 2022;36(8):905–19. <https://doi.org/10.1177/02698811221104054>. (Epub 2022 Jun 13. PMID: 35695604).
 37. Kannt A, Rajagopal S, Kadnur SV, Suresh J, Bhamidipati RK, Swaminathan S, Hallur MS, Kristam R, Elvert R, Czech J, Pfenninger A, Rudolph C, Schreuder H, Chandrasekar DV, Mane VS, Birudukota S, Shaik S, Zope BR, Burri RR, Anand NN, Thakur MK, Singh M, Parveen R, Kandan S, Mullangi R, Yura T, Gosu R, Ruf S, Dhakshinamoorthy S. A small molecule inhibitor of Nicotinamide N-methyltransferase for the treatment of metabolic disorders. *Sci Rep*. 2018;8:3660. <https://doi.org/10.1038/s41598-018-22081-7>. (PMID:29483571;PMCID:PMC5826917).
 38. Kopantzev EP, Monastyrskaya GS, Vinogradova TV, Zinoviyeva MV, Kostina MB, Filyukova OB, Tonevitsky AG, Sukhikh GT, Sverdlov ED. Differences in gene expression levels between early and later stages of human lung development are opposite to those between normal lung tissue and non-small lung cell carcinoma. *Lung Cancer*. 2008;62:23–34. <https://doi.org/10.1016/j.lungcan.2008.02.011>. (Epub 2008 Apr 3. PMID: 18394749).
 39. Kuehnelt D, Engström K, Skräöder H, Kokarnig S, Schlebusch C, Kippler M, Alhamdow A, Nermell B, Francesconi K, Broberg K, Vahter M. Selenium metabolism to the trimethylselenonium ion (TMSe) varies markedly because of polymorphisms in the indolethylamine N-methyltransferase gene. *Am J Clin Nutr*. 2015;102:1406–15. <https://doi.org/10.3945/ajcn.115.114157>. (Epub 2015 Nov 4. PMID: 26537946).
 40. Larkin SE, Holmes S, Cree IA, Walker T, Basketter V, Bickers B, Harris S, Garbis SD, Townsend PA, Aukim-Hastie C. Identification of markers of prostate cancer progression using candidate gene expression. *Br J Cancer*. 2012;106:157–65. <https://doi.org/10.1038/bjc.2011.490>. (PMID:22075945;PMCID:PMC3251845).
 41. Lindman S, Xue WF, Szczepankiewicz O, Bauer MC, Nilsson H, Linse S. Salting the charged surface: pH and salt dependence of protein G B1 stability. *Biophys J*. 2006;90:2911–21. <https://doi.org/10.1529/biophysj.105.071050>. (Epub 2006 Jan 27. PMID: 16443658; PMCID: PMC1414578).
 42. Liscombe DK, Louie GV, Noel JP. Architectures, mechanisms and molecular evolution of natural product methyltransferases. *Nat Prod Rep*. 2012;29(10):1238–50. <https://doi.org/10.1039/c2np20029e>. (Epub 2012 Aug 1. PMID: 22850796).
 43. López-Torres CD, Torres-Mena JE, Castro-Gil MP, Villa-Treviño S, Arellanes-Robledo J, Del Pozo-Yauner L, Pérez-Carreón JI. Downregulation of indolethylamine N-methyltransferase is an early event in the rat hepatocarcinogenesis and is associated with poor prognosis in hepatocellular carcinoma patients. *J Gene Med*. 2022;24: e3439. <https://doi.org/10.1002/jgm.3439>. (Epub 2022 Jul 24. PMID: 35816441).
 44. Luan CH, Light SH, Dunne SF, Anderson WF. Ligand screening using fluorescence thermal shift analysis (FTS). *Methods Mol Biol*. 2014;1140:263–89. https://doi.org/10.1007/978-1-4939-0354-2_20. (PMID: 24590724).
 45. Mandell AJ, Morgan M. Indole(ethyl)amine N-methyltransferase in human brain. *Nature*. 1971;230:85–7. <https://doi.org/10.1038/newbio230085a0>. (PMID: 5279043).
 46. Matulis D, Kranz JK, Salemm FR, Todd MJ. Thermodynamic stability of carbonic anhydrase: measurements of binding affinity and stoichiometry using ThermoFluor. *Biochemistry*. 2005;44:5258–66. <https://doi.org/10.1021/bi048135v>. (PMID: 15794662).
 47. Mavlyutov TA, Baker EM, Losenegger TM, Kim JR, Torres B, Epstein ML, Ruoho AE. The sigma-1 receptor—a therapeutic target for the treatment of ALS? *Adv Exp Med Biol*. 2017;964:255–65. https://doi.org/10.1007/978-3-319-50174-1_17. (PMID: 28315276).
 48. Mavlyutov TA, Epstein ML, Liu P, Verbny YI, Ziskind-Conhaim L, Ruoho AE. Development of the sigma-1 receptor in C-terminals of motoneurons and colocalization with the N, N'-dimethyltryptamine forming enzyme, indole-N-methyl transferase. *Neuroscience*. 2012;206:60–8. <https://doi.org/10.1016/j.neuroscience.2011.12.040>. (Epub 2012 Jan 4. PMID: 22265729; PMCID: PMC3321351).
 49. Meng EC, Goddard TD, Pettersen EF, Couch GS, Pearson ZJ, Morris JH, Ferrin TE. UCSF ChimeraX: tools for structure building and analysis. *Protein Sci*. 2023;32: e4792. <https://doi.org/10.1002/pro.4792>. (PMID:37774136;PMCID:PMC10588335).
 50. Murray RM, Oon MC, Rodnight R, Birley JL, Smith A. Increased excretion of dimethyltryptamine and certain features of psychosis: a possible association. *Arch Gen Psychiatry*. 1979;36(6):644–9. <https://doi.org/10.1001/archpsyc.1979.01780060034003>. (PMID: 286576).
 51. Neelakantan H, Vance V, Wang HL, McHardy SF, Watowich SJ. Noncoupled fluorescent assay for direct real-time monitoring of nicotinamide N-methyltransferase activity. *Biochemistry*. 2017;56:824–32. <https://doi.org/10.1021/acs.biochem.6b01215>. (Epub 2017 Jan 30. PMID: 28121423).
 52. Olsson TS, Williams MA, Pitt WR, Ladbury JE. The thermodynamics of protein-ligand interaction and solvation: insights for ligand design. *J Mol Biol*. 2008;384:1002–17. <https://doi.org/10.1016/j.jmb.2008.09.073>. (Epub 2008 Oct 9. PMID: 18930735).
 53. Peng Y, Sartini D, Pozzi V, Wilk D, Emanuelli M, Yee VC. Structural basis of substrate recognition in human nicotinamide N-methyltransferase. *Biochemistry*. 2011;50(36):7800–8. <https://doi.org/10.1021/bi2007614>. (Epub 2011 Aug 17. PMID: 21823666; PMCID: PMC3989893).
 54. Petrauskas V, Kazlauskas E, Gedgaudas M, Baranauskienė L, Zubrienė A, Matulis D. Thermal shift assay for protein-ligand dissociation constant determination. *TrAC, Trends Anal Chem*. 2024;170: 117417. <https://doi.org/10.1016/j.trac.2023.117417>.
 55. Petukhova VZ, Aboagye SY, Ardini M, Lullo RP, Fata F, Byrne ME, Gabriele F, Martin LM, Harding LNM, Gone V, Dangi B, Lantvit DD, Nikolic D, Ippoliti R, Effantin G, Ling WL, Johnson JJ, Thatcher GR, Angelucci F, Williams DL, Petukhov PA. Non-covalent inhibitors of thioredoxin glutathione reductase with schistosomicidal activity in vivo. *Nat Commun*. 2023;14:3737. <https://doi.org/10.1038/s41467-023-39444-y>. (PMID:37349300;PMCID: PMC10287695).
 56. Räisänen M, Kärrkäinen J. Quantitative assay of the N-methylated metabolites of tryptamine and serotonin by gas chromatography mass spectrometry as applied to the determination of lung indolethylamine N-methyltransferase activity. *Biomed Mass Spectrom*. 1978;5:596–600. <https://doi.org/10.1002/bms.1200051010>. (PMID: 284808).
 57. Richter M. Functional diversity of organic molecule enzyme cofactors. *Nat Prod Rep*. 2013;30:1324–45. <https://doi.org/10.1039/C3NP70045C>. (Epub 2013 Aug 12. PMID: 23934236).
 58. Sievers F, Wilm A, Dineen DG, Gibson TJ, Karplus K, Li W, Lopez R, McWilliam H, Remmert M, Söding J, Thompson JD, Higgins D. Fast, scalable generation of high-quality protein multiple sequence alignments using Clustal Omega. *Mol Sys Biol*. 2011;7:539. <https://doi.org/10.1038/msb.2011.75>. (PMID: 21988835; PMCID: PMC3261699).
 59. Sledz P, Lang S, Stubbs CJ, Abell C. High-throughput interrogation of ligand binding mode using a fluorescence-based assay. *Angew Chem Int Ed Engl*. 2012;51:7680–3. <https://doi.org/10.1002/anie.201202660>.
 60. Melnyk S, Pogribna M, Pogribny IP, Yi P, James SJ. Measurement of plasma and intracellular S-adenosylmethionine and S-adenosylhomocysteine utilizing coulometric electrochemical detection: alterations with plasma homocysteine and Pyridoxal 5'-phosphate concentrations. *Clin Chem*. 2000;46(2):265–72. <https://doi.org/10.1093/clinchem/46.2.265>. (Erratum. In: *Clin Chem* 2001 Mar; 47(3):612. PMID: 10657384).

61. Strahilevitz M, Narasimhachari N, Fischer GW, Meltzer HY, Himwich HE. Indolethylamine-N-methyltransferase activity in psychiatric patients and controls. *Biol Psychiatry*. 1975;10:287–302 (PMID: 1139013).
62. Swaminathan S, Birudukota S, Thakur MK, Parveen R, Kandan S, Juluri S, Shaik S, Anand NN, Burri RR, Kristam R, Hallur MS, Rajagopal S, Schreuder H, Langer T, Rudolph C, Ruf S, Dhakshinamoorthy S, Gosu R, Kannt A. Crystal structures of monkey and mouse nicotinamide N-methyltransferase (NNMT) bound with end product, 1-methyl nicotinamide. *Biochem Biophys Res Commun*. 2017;491(2):416–22. <https://doi.org/10.1016/j.bbrc.2017.07.087>. (Epub 2017 Jul 15 PMID: 28720493).
63. Swaminathan S, Theerthan AL. Protein Stability Using Thermal Shift Assay (TSA): pH Tolerance. In: Zaheer SM, Gosu R. (eds) *Methods for Fragments Screening Using Surface Plasmon Resonance*. 2021, Springer, Singapore; https://doi.org/10.1007/978-981-16-1536-8_5
64. Tanaka YK, Takata A, Takahashi K, Yamagishi Y, Fukumoto Y, Suzuki N, Ogra Y. Thiopurine S-methyltransferase- and indolethylamine N-methyltransferase-mediated formation of methylated tellurium compounds from tellurite. *Arch Toxicol*. 2025;99:237–44. <https://doi.org/10.1007/s00204-024-03890-4>. (Epub 2024 Oct 17. PMID: 39417876; PMCID: PMC11742336).
65. Thompson MA, Moon E, Kim UJ, Xu J, Siciliano MJ, Weinshilboum RM. Human indolethylamine N-methyltransferase: cDNA cloning and expression, gene cloning, and chromosomal localization. *Genomics*. 1999;61(3):285–97. <https://doi.org/10.1006/geno.1999.5960>. (PMID: 10552930).
66. Thompson MA, Weinshilboum RM. Rabbit lung indolethylamine N-methyltransferase. cDNA and gene cloning and characterization. *J Biol Chem*. 1998;273(51):34502–10. <https://doi.org/10.1074/jbc.273.51.34502>. (PMID: 9852119).
67. Tokmakov AA, Kurotani A, Sato KI. Protein pl and intracellular localization. *Front Mol Biosci*. 2021;8: 775736. <https://doi.org/10.3389/fmolb.2021.775736>. (PMID:34912847;PMCID:PMC8667598).
68. Torres B, Tyler JS, Satyshur KA, Ruoho AE. Human indole(ethyl)amine-N-methyltransferase (hINMT) catalyzed methylation of tryptamine, dimethylsulfide and dimethylselenide is enhanced under reducing conditions—a comparison between 254C and 254F, two common hINMT variants. *PLoS One* 2019, 14:e0219664; <https://doi.org/10.1371/journal.pone.0219664>. Erratum for: *PLoS One*. 2019 Jul 16; 14(7):e0219664; <https://doi.org/10.1371/journal.pone.0219664>. PMID: 31574131; PMCID: PMC6772043
69. Vivoli M, Novak HR, Littlechild JA, Harmer NJ. Determination of protein-ligand interactions using differential scanning fluorimetry. *J Vis Exp*. 2014;91: e51809. <https://doi.org/10.3791/51809>. (PMID:25285605;PMCID:PMC4692391).
70. Witek MA, Kuiper EG, Minten E, Crispell EK, Conn GL. A novel motif for S-adenosyl-L-methionine binding by the ribosomal RNA methyltransferase TlyA from mycobacterium tuberculosis. *J Biol Chem*. 2017;292:1977–87. <https://doi.org/10.1074/jbc.M116.752659>. (Epub 2016 Dec 27. PMID: 28031456; PMCID: PMC5290967).
71. Wu T, Hornsby M, Zhu L, Yu JC, Shokat KM, Gestwicki JE. Protocol for performing and optimizing differential scanning fluorimetry experiments. *STAR Protoc*. 2023;4:102688. <https://doi.org/10.1016/j.xpro.2023.102688>.
72. Zhang AA, He QL, Zhao Q. Mining and Characterization of Indolethylamine N-Methyltransferases in Amphibian Toad *Bufo gargarizans*. *Biochemistry*. 2023;62(16):2371–81. <https://doi.org/10.1021/acs.biochem.3c00229>

Publisher's Note

Springer Nature remains neutral with regard to jurisdictional claims in published maps and institutional affiliations.